RESEARCH ARTICLE

Gaussian and non-Gaussian inverse modeling of groundwater flow using copulas and random mixing

András Bárdossy[1] and Sebastian Hörning[1]

[1]Institute for Modelling Hydraulic and Environmental Systems, University of Stuttgart, Stuttgart, Germany

Abstract This paper presents a new copula-based methodology for Gaussian and non-Gaussian inverse modeling of groundwater flow. The presented approach is embedded in a Monte Carlo framework and it is based on the concept of mixing spatial random fields where a spatial copula serves as spatial dependence function. The target conditional spatial distribution of hydraulic transmissivities is obtained as a linear combination of unconditional spatial fields. The corresponding weights of this linear combination are chosen such that the combined field has the prescribed spatial variability, and honors all the observations of hydraulic transmissivities. The constraints related to hydraulic head observations are nonlinear. In order to fulfill these constraints, a connected domain in the weight space, inside which all linear constraints are fulfilled, is identified. This domain is defined analytically and includes an infinite number of conditional fields (i.e., conditioned on the observed hydraulic transmissivities), and the nonlinear constraints can be fulfilled via minimization of the deviation of the modeled and the observed hydraulic heads. This procedure enables the simulation of a great number of solutions for the inverse problem, allowing a reasonable quantification of the associated uncertainties. The methodology can be used for fields with Gaussian copula dependence, and fields with specific non-Gaussian copula dependence. Further, arbitrary marginal distributions can be considered.

1. Introduction

Modeling of groundwater flow is important for a number of different tasks, such as groundwater management and contaminant remediation. The mathematical models describing groundwater flow are based on the continuity equation and Darcy's law and are formulated in the form of partial differential equations. These equations require the knowledge of parameters such as hydraulic transmissivity and porosity. These parameters, as they describe natural conditions below the surface, cannot be assessed directly. Their values are estimated from a limited number of point measurements (wells) and sometimes combined with information obtained from indirect observations such as geophysics. This limited information is the basis for the estimation of the parameters over the whole investigation area. There are a great number of geostatistical methods that can be used to estimate spatial fields conditioned on a limited number of observations. These methods, however, are only partially useful for groundwater modeling. The reason for this is that in addition to the observations of the parameters, groundwater heads are also observed at a number of locations. These groundwater heads are linked to the partly unknown parameters (transmissivities). The link is established through a mathematical model of groundwater flow formulated as partial differential equations. Thus, these head observations can be used as information for reducing the uncertainty of the transmissivities. This is, however, a complicated task as the link between heads and the other parameters is not linear.

The task to estimate the unknown transmissivities from limited hydraulic transmissivity and groundwater head observations is the typical inverse problem in groundwater modeling. Other inverse problems formulated using concentrations of different substances or transient conditions can also be treated with the suggested methodology. Inverse modeling is usually an ill-posed problem: either there is no solution (contradicting constraints) or there are infinitely many solutions. Furthermore, specific properties of the distribution—such as nonnegativity of the values constitute further problems [*Michalak*, 2008]. The complexity of the problem seldom allows an exact solution, instead a solution which is close to the observations is attempted. These problems are usually formulated as optimization problems. The objective function(s) are related to the observations and to the spatial structure of the field. The unknown field is usually represented

by a dense grid containing a large number of points. Thus, a straightforward optimization is computationally not feasible. Therefore, a reduction of the dimensions of the problem is absolutely necessary.

There are a great number of different methods ranging from manual model calibration to sophisticated numerical procedures that can be used for this problem, e.g., the pilot point method [*RamaRao et al.*, 1995], the ensemble Kalman filter [*Evensen*, 2003; *Hendricks Franssen and Kinzelbach*, 2008; *Zhou et al.*, 2011, 2012a], the self-calibration method [*Gómez-Hernández et al.*, 1997; *Franssen et al.*, 2003], the Markov chain Monte Carlo method [*Oliver et al.*, 1997; *Fu and Gómez-Hernández*, 2008], or the gradual deformation approach [*Hu*, 2000; *Hu et al.*, 2001; *Hu*, 2002; *Caers*, 2003]. A comprehensive review of several methods is given in *Zhou et al.* [2014] and a comparison of different methods can be found in *Franssen et al.* [2009].

Another important issue in groundwater modeling is whether the hydraulic transmissivities exhibit a Gaussian spatial dependence structure or not. Most inverse modeling methods implicitly assume multi-Gaussianity, however, not only the marginal distributions but also the spatial dependence of the hydraulic transmissivity field $W(x)$ might differ significantly from Gaussian. Such non-Gaussian spatial structures have a significant influence on groundwater flow and transport behavior. *Gómez-Hernández and Wen* [1998] showed how different non-Gaussian models, all sharing the same marginals and the same covariance function but with different spatial patterns of continuity, lead to different groundwater travel times. In *Zinn and Harvey* [2003], the effect of non-Gaussian spatial dependence on groundwater flow and mass transfer was demonstrated using several examples. In *Haslauer et al.* [2012], it was shown for a selected case study that spatial dependence of transmissivities can best be modeled using a v-transformed copula. In *Guthke* [2013] it was shown how different real-world processes lead to asymmetric spatial dependence structures which can be described using copulas. In general, a Gaussian spatial dependence implies a low spatial correlation of extremes, however, the dependence of transmissivities is often asymmetrical—high values being clustered differently than the low values. Some inverse modeling methods are able to handle non-Gaussian patterns of variability. However, most of them are based on multiple-point geostatistics, i.e., they require a suitable training image.

Most methods, practically all of them that use only moments up to the order 2, can only handle Gaussian spatial patterns. But there is an increasing interest in inverse modeling approaches that are able to deal with non-Gaussian dependencies. However, from the above mentioned techniques, only the Markov chain Monte Carlo method, extensions of the gradual deformation method, and modified ensemble Kalman filter approaches [*Jafarpour and Khodabakhshi*, 2011; *Zhou et al.*, 2011] are able to handle certain types of non-Gaussian patterns. A different approach to address non-Gaussianity is to use multiple-point geostatistics, where a training image serves as a conceptual geological model [*Guardiano and Srivastava*, 1993]. Several multiple-point geostatistics algorithms are available, e.g., SNESIM [*Strebelle*, 2002], FILTERSIM [*Zhang et al.*, 2006], SIMPAT [*Arpat and Caers*, 2007], or direct sampling [*Mariethoz et al.*, 2010]. In the context of inverse modeling, multiple-point geostatistics are frequently applied [*Caers and Hoffman*, 2006; *Ronayne et al.*, 2008; *Alcolea and Renard*, 2010; *Zhou et al.*, 2012b; *Hu et al.*, 2013] and the advantages of multiple-point geostatistics compared to variogram-based methods have been confirmed in several studies [*Journel and Zhang*, 2006; *Huysmans and Dassargues*, 2010]. However, all the methods referred to above suffer from one main drawback, namely the training image itself. In general, a training image is a conceptual model and its preparation is often based on subjective criteria of the modeling expert [*Pérez et al.*, 2014]. Thus, the selection of an appropriate training image is a main issue, especially in 3-D applications.

In this paper, a new methodology based on random mixing of spatial fields is presented. It is an extension of the methodology for the gradual deformation of Gaussian random fields described in *Hu* [2000]. The purpose of the new method is to produce fields that not only reproduce the spatial variability of the field but also the hydraulic transmissivity measurements, other linear functions related to transmissivities, and the corresponding head values. The proposed method uses the concept of spatial copulas, thus Gaussianity and non-Gaussianity in both, the marginal distribution as well as in the spatial dependence can be considered. The occurrence of non-Gaussian (and non-logGaussian) distributions in permeability fields was investigated in *Riva et al.* [2013]. The copula-based approach can accommodate arbitrary heavy tailed marginals. The copula serves as spatial dependence function which is fitted to the observations directly, hence non-Gaussianity of the dependence can be addressed without the need for a suitable training image. However, the suggested approach can be coupled to a multiple-point geostatistics method which allows inversion under specific structural constraints.

The basic assumptions and the basics of copulas are introduced in section 2. Their use corresponding to the suggested approach as well as the approach itself is described in section 3. This section also contains the extensions to non-Gaussian spatial copulas. In section 4, the numerical methodology is described, and in section 5, the suggested inverse modeling approach is demonstrated using several examples. Conclusions are drawn in section 6.

2. Basic Assumptions, and the Application of Spatial Copulas

Assuming that $W(x)$ is the unknown hydraulic transmissivity field with x being the location in the investigation domain D, the general goals of inverse modeling are as follows:

1. To find a field $W(x)$ for $x \in D$ with the observed distribution and spatial variability.
2. To honor all observations at locations x_t of the hydraulic transmissivities in field $W(x)$ such that $W(x_t)=w_t$ for $t=1,\ldots,T$.
3. To have the head field $H_W(u)$, corresponding to the field $W(x)$ and calculated from the corresponding differential equation with given boundary and initial conditions with the observations at locations u_m, fulfilling $H_W(u_m)=h_m$ for $m=1,\ldots,M$.

There are different possibilities to describe spatial variability. The most common assumptions are second-order stationarity or an explicit assumption of a multivariate lognormal distribution of the spatial field. The assumption of a multivariate lognormal spatial distribution is very restrictive, and statistical investigations of observed data provide evidence of its unsuitability [*Gómez-Hernández and Wen*, 1998; *Haslauer et al.*, 2012]. Therefore, models which allow non-Gaussian marginals and/or non-Gaussian dependence are required. Multipoint geostatistics and indicator geostatistics offer different approaches, which allow certain types of non-Gaussian dependence. Copulas offer another possibility to define model with non-Gaussian properties. The multivariate lognormal case can also be simulated using copulas. The approach allows the consideration of arbitrary marginal distributions with both Gaussian and certain non-Gaussian spatial dependencies. For the sake of completeness, the copula-based methodology to describe spatial variability is briefly sketched here. For more details on spatial copulas and on copula parameter estimation based on maximum likelihood, see *Bárdossy* [2006] and *Bárdossy and Li* [2008].

In general, copulas are multivariate distributions defined on the unit hypercube with uniform univariate marginals. Formally:

$$C : [0,1]^n = [0,1] \tag{1}$$

for any number $0 \le u_i \le 1$:

$$C(u^{(i)})=u_i \quad if \quad u^i=(1,\ldots,1,u_i,1,\ldots,1) \tag{2}$$

Copulas are used to describe the dependence between random variables independently of their marginal distributions, i.e., monotonic transformations of the marginals do not influence the dependence structure. They are linked to multivariate distributions by Sklar's theorem [*Sklar*, 1959] that proves that each continuous multivariate distribution $F(x_1,\ldots,x_n)$ can be represented with the help of a unique copula:

$$F(x_1,\ldots,x_n)=C(F_{x_1}(x_1),\ldots,F_{x_n}(x_n)) \tag{3}$$

where $F_{x_i}(x)$ denotes the ith one-dimensional marginal distribution of the multivariate distribution. Vice versa, any copula C can be used to create a multivariate distribution $F(x_1,\ldots,x_n)$.

Copulas of multivariate distributions can be extracted by taking:

$$C(u_1,\ldots,u_n)=F(F_{x_1}^{-1}(u_1),\ldots,F_{x_n}^{-1}(u_n)) \tag{4}$$

The major advantage in using copulas for describing multivariate distributions is that the dependence structure can be modeled separately from the marginal distributions. For more information on copulas, the interested reader is referred to *Nelson* [1999].

In the geostatistical context, copulas can be used to describe the joint multivariate distribution corresponding to variables that are spatially distributed in the domain of interest. As in traditional geostatistics, it is

assumed that the univariate marginal distribution corresponding to each point of the domain is the same, and the spatial dependence is translation invariant, thus for any separating vector h. This means that for any set of points s_i in the investigation domain such that $s_i + h$ is also in the domain the spatial copula of the multivariate distribution is such that:

$$
\begin{aligned}
C_S(u_1, \ldots, u_k) &= P(F_Z(Z(s_1)) < u_1, \ldots, F_Z(Z(s_k)) < u_k) \\
&= P(F_Z(Z(s_1 + h)) < u_1, \ldots, F_Z(Z(s_k + h)) < u_k) \\
&= C_{S+h}(u_1, \ldots, u_k)
\end{aligned}
\tag{5}
$$

Spatial copulas have to fulfill certain conditions which are listed in *Bárdossy* [2006].

The most common spatial copula is the Gaussian copula obtained by applying (4) for the multivariate normal distribution. A class of non-Gaussian copulas can be obtained by a nonmonotonic transformation of the multivariate normal distribution.

If $Z(x)$ is a Gaussian random field defined on a selected domain, then

$$
V(x) = g(Z(x))
\tag{6}
$$

defines a new random field which is non-Gaussian if $g(z)$ is a nonmonotonic function. If $g(z)$ is continuous then the copula of $V(x)$ obtained using (4) fulfills the conditions of a spatial copula. An example for this is the v-copula used in *Bárdossy and Li* [2008] with:

$$
g(z) = \begin{cases} k(z-m) & \text{if } z \geq m \\ m-z & \text{if } z < m \end{cases}
\tag{7}
$$

In *Bárdossy and Li* [2008], parameter inference for such copulas is described. *Haslauer et al.* [2012] showed that for the Borden site such a copula provides a better description of spatial variability as the Gaussian copula, and that contaminant transport is significantly influenced by the choice of the spatial copula.

In Figure 1, two realization of random fields are shown. The two fields have the same marginal distribution and the same variogram. The difference of the spatial structure of the two fields can be diagnosed by their different bivariate spatial copulas. The two fields were generated as common random fields [*Guthke and Bárdossy*, 2012] in order to make a clearer distinction between the structures possible.

3. Methodology: Simulation and Inverse Modeling

Inverse modeling is often formulated as an optimization problem, where a transmissivity field with given spatial variability is to be found minimizing the difference between observed and simulated transmissivity and corresponding head values. This problem can effectively be solved restricting the search domain to a connected set of fields with the given spatial variability which honor the observation. Such a technique, called gradual deformation, was developed in *Hu* [2000]. The methodology is modified in order to cope with more general linear constraints. The nonlinear constraints imposed by the flow model can be fulfilled by an unconstrained minimization of the squared differences.

In this paper, inverse modeling using two different spatial copula models of spatial dependence of the transmissivity field $W(x)$ is presented. First, the Gaussian copula-based methodology is described which enables the use of any arbitrary marginal distribution with multi-Gaussian spatial dependence structure. Second, the copula defined by (7) leading to a non-Gaussian spatial dependence and with an arbitrary marginal is considered. This allows asymmetric dependencies of the values and different structures of spatial connectedness.

3.1. Gaussian Copulas

In groundwater modeling, it is often assumed that the hydraulic transmissivities follow a multivariate lognormal distribution [*Freeze*, 1975]. However, the distribution of the transmissivity values does not necessarily follow the lognormal distribution. The use of Gaussian copulas allows the consideration of the multivariate lognormal distribution and that of a non-lognormal marginal with a Gaussian dependence. The Gaussian copula is defined in accordance with (4) as
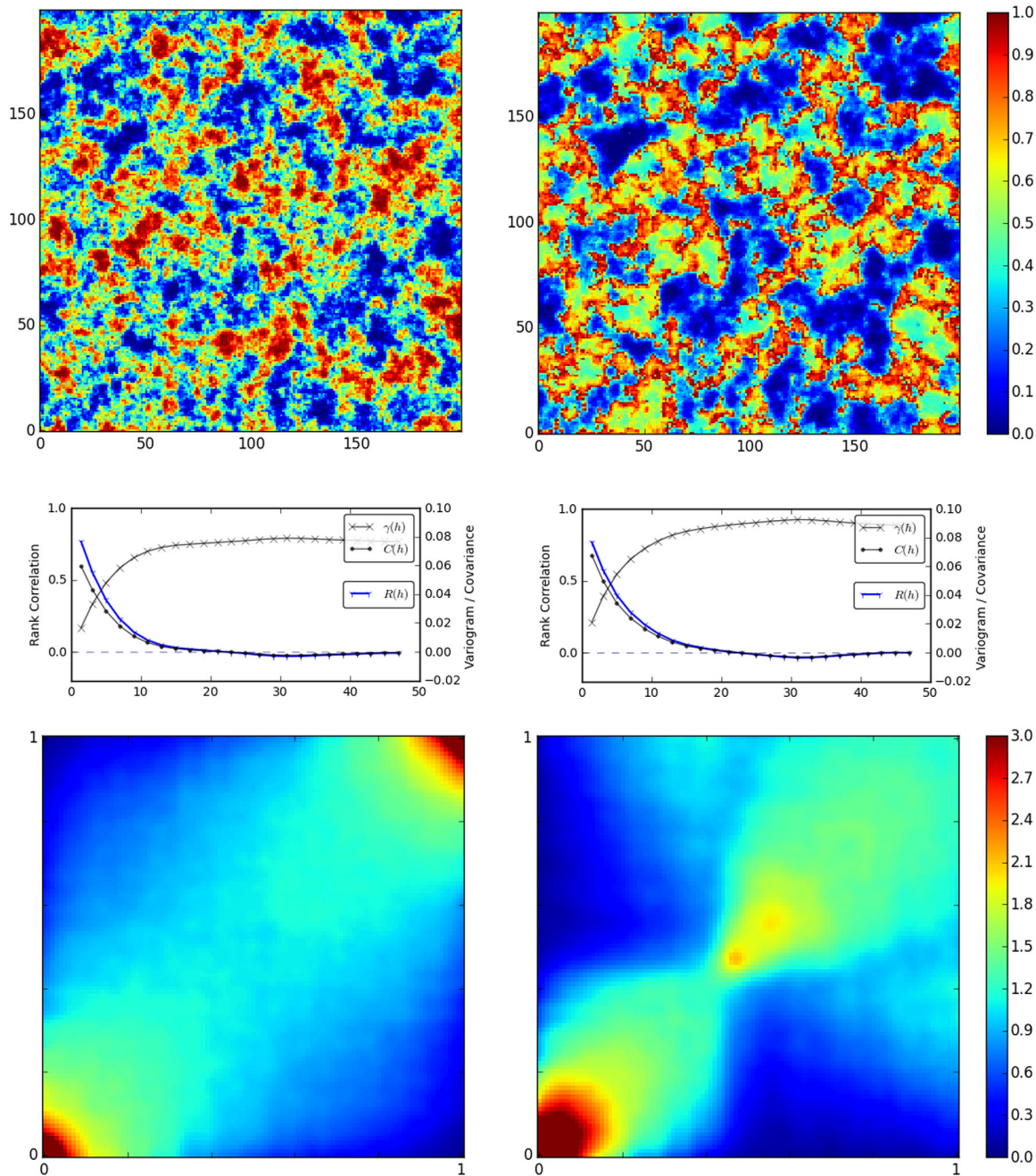
Figure 1. Common random field with (left) Gaussian and (right) non-Gaussian dependence structure.

$$C_\Gamma(u_1, \ldots, u_n) = \Phi_{\Gamma,n}(\Phi^{-1}(u_1), \ldots, \Phi^{-1}(u_n)) \qquad (8)$$

where Φ^{-1} denotes the inverse univariate standard normal distribution and $\Phi_{\Gamma,n}$ the n-dimensional Gaussian distribution with correlation matrix Γ and standard normal marginals. The transformation:

$$Z(x) = \Phi^{-1}(F(W(x))) \qquad (9)$$

applied for each location x of the field under investigation transforms the hydraulic transmissivity field W to a multinormal field Z. Note that the covariance of Z in the normal space is different from the covariance of W. Then the conditional simulation of the field Z is carried out using a linear combination of unconditional fields as described below. Finally, the conditional field Z is transformed back to W for each point x via:

$$W(x) = F^{-1}(\Phi(Z(x))) \tag{10}$$

where F^{-1} denotes the inverse marginal distribution of $W(x)$. Thus, the transmissivity field $W(x)$ exhibits a Gaussian spatial dependence structure with an arbitrary marginal distribution $F(W(x))$, which includes the classical lognormal case. In the next section, the simulation of the field $W(x)$ is described.

3.2. Linear Conditions

In order to find a possible solution to the inverse problem, the first step is to identify fields with the prescribed spatial dependence expressed by the correlation matrix Γ of the copula introduced in (8) and with the prescribed values (transformed hydraulic transmissivities) at the observation locations. Let Z be the transformed multinormal field obtained from the transformation described above. This random field Z is expressed as a linear combination of other unconditional random fields Y_i. This means:

$$Z = \sum_{i=1}^{n} \alpha_i Y_i \tag{11}$$

Let Y_i for $i=1,\ldots,n$ be independent random fields with zero expectation, unit variance, and the correlation matrix being the same Γ as of Z. Such fields can be simulated using different methods such as Fast Fourier Transformation for regular grids [*Dietrich and Newsam*, 1996], Turning band simulation [*Journel*, 1974], or the Cholesky transformation of the covariance matrix.

As described in *Hu* [2000], if all Y_i have the same covariance matrix Γ and:

$$\sum_{i=1}^{n} \alpha_i^2 = 1 \tag{12}$$

then Z also has the same covariance structure as all random fields Y_i.

The conditional field Z should honor certain linear constraints:

$$\mathbf{A}_t(Z) = z_t \quad t=1,\ldots,T \tag{13}$$

where $\mathbf{A}_t(Z)$ represent linear functions on Z. They include as special case point and/or integral observations (for a point x_j the linear function is $\mathbf{A}(Z) = Z(x_j)$).

In *Hu* [2000], *Hu et al.* [2001] point observations are incorporated using conditioning via Kriging. In *Hu* [2002], the methodology is extended to combine dependent conditional realizations. The approach suggested here incorporates any linear constraint directly. Therefore, for the n independent realizations of unconditional fields Y_i, the weights α_i have to be selected so that:

$$\mathbf{A}_t\left(\sum_{i=1}^{n} \alpha_i Y_i\right) = \sum_{i=1}^{n} \alpha_i \mathbf{A}_t(Y_i) = z_t \quad t=1,\ldots,T \tag{14}$$

If the number n of fields Y_i is greater than T there are weights α_i that fulfill (14). However, these weights do not necessarily fulfill (12). Thus, the next step is to find weights that fulfill both (14) and (12). If the dimension $n > T$, the weights in (14) are nonunique. These weights form a hypersurface in the n-dimensional space of the weights $(\alpha_1,\ldots,\alpha_n)$. If (in the n-dimensional space of weights) this hypersurface intersects with the unit sphere then one can find a solution. The intersection is not empty if and only if the closest point of the hypersurface to the origin is within the unit sphere. This closest point (minimizing the norm $\sum_{i=1}^{n} \alpha_i^2$) can be found for any set of fields Y_i by singular value decomposition [*Golub and Kahan*, 1965]. By increasing n (adding further random fields Y_i) the norm can be reduced below 1.

In order to find a solution which also fulfills (12) and which honors nonlinear constraints a component fulfilling the homogeneous conditions, that is, $\mathbf{A}_t(Y(\lambda)) = 0 \quad t=1,\ldots,T$ has to be added. This can be performed by solving the homogeneous equations using different additional unconditional fields V_{n+j} which share the same spatial properties as the fields Y_i:

$$\sum_{i=1}^{n} \beta_{j,i} \mathbf{A}_t(V_i) = -\mathbf{A}_t(V_{n+j}) \quad t=1,\dots,T \tag{15}$$

By solving (15) for a set of fields $j=1,\dots,N$, one obtains weights $(\beta_{j,1},\dots,\beta_{j,n},0,\dots,0,1,0,\dots,0)$ with 1 being at the $(n+j)$ th position, which are all solutions of the homogeneous equations. Linear combinations of these weights define fields $Y(\lambda)$ which also fulfill the homogeneous conditions:

$$Y(\lambda) = \sum_{j=1}^{N} \lambda_j \sum_{i=1}^{n+N} \beta_{j,i} V_i \tag{16}$$

The coefficients λ_j of the linear combination are arbitrary real numbers used as unknowns for an optimization procedure to honor nonlinear constraints. The final conditional field can now be obtained via:

$$Z_\lambda = \sum_{i=1}^{n} \alpha_i Y_i + k(\lambda) Y(\lambda) \tag{17}$$

where $k(\lambda)$ denotes a normalizing constant defined as

$$k(\lambda) = \pm \sqrt{\frac{1 - \sum_{i=1}^{n} \alpha_i^2}{\sum_{j=1}^{N} \left(\sum_{i=1}^{n+N} \beta_{j,i} \lambda_j\right)^2}} \tag{18}$$

which is required for the fulfillment of condition (12). If the deviation between observed and modeled head is not small enough, then an additional field V_{n+N+1} is generated, and the optimization (with respect to the λ values) is repeated. Note that the optima improve by adding a new field, and that the previous optimal solution can be taken as initial point for the next.

This method differs from the approach described in *Hu et al.* [2001] as

1. it does not require any Kriging for conditioning;
2. it allows the consideration of any kind of linear constraints (including point and block observations and correlations to external fields);
3. the optimization procedure used to fulfill nonlinear constraints such as the hydraulic heads for inverse modeling is unconditional; and
4. arbitrary marginal distribution can be used.

This construct has the specific advantage with respect to other linear conditioning methods, that using the points of the solution hyperplane it can be used to generate an infinite number of conditional fields.

3.3. Conditioning on the Head Observations
For each conditional hydraulic transmissivity field $W(x)$ obtained from the corresponding $Z(x)$, the solution of the groundwater flow equations provides calculated head $H_Z(u_m)$ values at the head observations. These are, unfortunately, usually different from the observed values h_m. Due to the nonlinear correspondence between $Z(x)$ and $W(x)$ described by the partial differential equation, these conditions cannot be considered as linear. As a next step, fields which also honor these conditions have to be found. The nonlinear constraints concerning the head observations can now be considered as

$$\sum_{m=1}^{M} \left(H_{Z_\lambda}(u_m) - h_m\right)^2 \rightarrow \min \tag{19}$$

an optimization problem with λ_j values $j=1,\dots,N$ being the unknowns, with no constraints. This is a standard continuous unconstrained optimization problem with m unknown λ_j values which can be solved by standard numerical procedures. If the solution is such that the deviation of the simulated heads from the observed is not greater than a selected threshold δ:

$$\sum_{m=1}^{M} (H_{Z_\lambda}(u_m) - h_m)^2 < \delta \tag{20}$$

then the solution is accepted, otherwise N is increased. The minimum of the objective function decreases as N, the number of additional fields considered, increases. Thus, step-by-step, a better solution can be obtained until the objective function becomes small enough, meaning that the head constraints are sufficiently fulfilled. Other objective functions such as consideration of the covariances of the head observations:

$$(H_{Z_\lambda}(u_m) - h_m)^T \Sigma (H_{Z_\lambda}(u_m) - h_m) < \delta \tag{21}$$

or the minimization of the maximal deviation:

$$\max_m |H_{Z_\lambda}(u_m) - h_m| < \delta \tag{22}$$

can alternatively be considered.

Note that for each choice of the random fields Y_i, a different solution of the problem can be obtained. Thus, this procedure can be used to produce an arbitrary number of random solutions of the inverse problem.

3.4. Non-Gaussian Dependence

The conditional simulation of fields with non-Gaussian copula-based spatial structures requires a few adjustments of the above described approach.

1. The univariate marginal distribution $G(v)$ of $g(Z(x))$, where $Z(x)$ is a univariate random variable with a Gaussian distribution is assessed. Depending on the form of g, this can be done either analytically or numerically.
2. The observed hydraulic transmissivity values $W(x)$ are transformed to the above distribution by

$$V(x_i) = G^{-1}(F(W(x_i))) \tag{23}$$

   where G^{-1} denotes the inverse univariate marginal distribution of $g(Z)$ and $F(W(x_i))$ denotes the marginal distribution of the observed values.

3. These $V(x)$ values are transformed back to the standard normal distribution using a Markov chain Monte Carlo (MCMC) approach. Here the Metropolis algorithm is used [*Hastings*, 1970]. This procedure is needed as the transformation is nonmonotonic. This means that a sample $Z(x_1), \dots, Z(x_n)$ is generated so that

$$V(x_i) = g(Z(x_i)) \tag{24}$$

   The density used for the Markov chain Monte Carlo simulation corresponding to this sample is $\Phi_n(Z(x_1), \dots, Z(x_n), \Gamma)$. Here Γ denotes the covariance matrix of $Z(x)$ and Φ_n denotes the n-dimensional Gaussian density. In the case of the v-transformed copula for each value $V(x_i)$, there are two *inverses* $Z(x_i)$ values which satisfy (24). They are $Z(x_i) = V(x_i)/k + m$ and $Z(x_i) = m - V(x_i)$. In the MCMC procedure, first the nonunique inverse is selected at random. Then the MCMC procedure is carried out by randomly changing one of the *inverses* using the density of the corresponding Z. The procedure is restarted for each realization. The number of MCMC steps is selected so that the result becomes independent from the initial realization. As the calculation of the density is simple the computational cost of it is low.
4. The conditional simulation of the field $Z(x)$ is carried out as described in section 3.2 for all point equality constraints. Note that those constraints are the sampled values $Z(x_1), \dots, Z(x_n)$ resulting from step 3.
5. The resulting conditional field $Z(x)$ is transformed back to $W(x)$ via:

$$W(x) = F^{-1}(G(g(Z(x)))) \tag{25}$$

   Here F^{-1} denotes the inverse marginal distribution of the observed values $W(x)$.

Thus, $W(x)$ exhibits a non-Gaussian spatial dependence structure defined by the nonmonotonic transformation (7). Furthermore, $F(W(x))$ is an arbitrary marginal distribution.

3.5. Combination With Known Geological Structure Information

It is often assumed that the hydraulic transmissivity field is structured in a specific way according to the geological processes leading to these variables. For example, geological sedimentation processes could lead to fluvial deposits, i.e., contrasting facies of highly different transmissivities. Such structures are often

obtained by combining observations and training images. In *Li et al.* [2012], a Kalman filter based method is suggested for inverse modeling for this case. Here a different approach is presented.

Structural information obtained from training images can be combined with the random mixing methodology to solve the inverse problem. The inversion is carried out for each realization of the categorical field. Assume that a conditional categorical map has been obtained using multipoint geostatistics [*Strebelle*, 2002; *Mariethoz et al.*, 2010]. This means that a random field $B(x)$ with possible values $B(x)=1,\ldots,B$ is obtained for conditioning. For each of the possible classes b, there can be a different distribution of the hydraulic transmissivity values:

$$F_b(w)=P(W(x) < w|B(x)=b) \tag{26}$$

An inverse solution for the problem with the above additional condition can be obtained by defining the new field:

$$Z(x)=\Phi^{-1}(F_b(W(x))) \tag{27}$$

This $Z(x)$ can then be treated the same way as described in section 3.2. Note that here it is assumed that the spatial variability within the different units b is the same in the rank sense, and that there is a kind of continuity in the fields. This assumption could be weakened, by allowing an individual field $Z_b(x)$ for each geological unit b, with a specific description of the spatial variability. In this case, the fields are mixed simultaneously, the same way as described above.

The likelihood of the field $B(x)$ can be estimated via the likelihood of the realizations $Z_b(x)$, and an Monte Carlo Markov chain approach may provide means to perform combined simulations. This however requires more research and goes beyond the scope of this paper.

4. Numerical Methodology

As described above, a conditional realization of the hydraulic transmissivities is determined by a linear combination of unconditional Gaussian random fields. Thus, a large number of Gaussian random fields could be required. In order to reduce the computational burden, simulation on a regular grid using Fast Fourier Transformation [*Wood and Chan*, 1994; *Wood*, 1995; *Dietrich and Newsam*, 1996] is adopted for all examples. This method allows very fast simulation of unconditional Gaussian random fields.
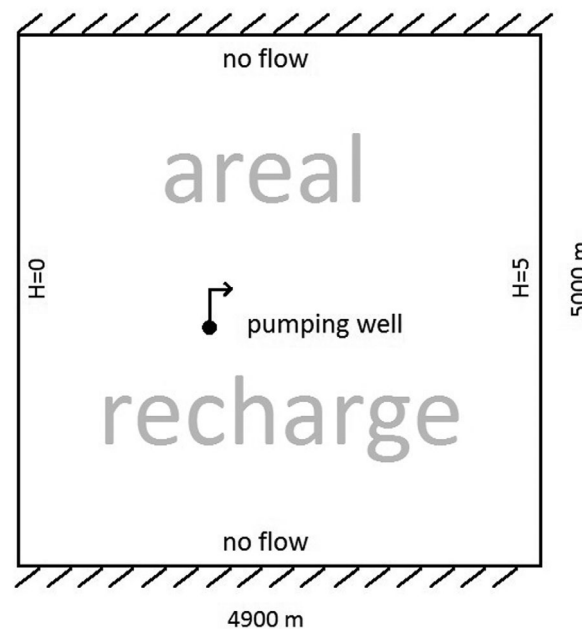

Figure 2. General flow setup for the synthetic test case.

According to section 3.3, the inverse problem is transformed to a continuous optimization problem. Hence, every continuous optimization technique can be applied. Throughout this paper, the *COBYLA* algorithm (constrained optimization by linear approximation) is adopted. This algorithm is based on linear approximations of the objective function and each constraint. For further details, the reader is referred to *Powell* [1998].

The numerical flow and transport model applied is *HydroGeosphere* [*Therrien and Sudicky*, 1996]. *HydroGeosphere* is a three-dimensional numerical model describing fully integrated subsurface and surface flow and solute transport. A finite element steady state scheme is adopted throughout this paper.

5. Applications

The suggested inverse modeling approach is demonstrated using several examples. To avoid
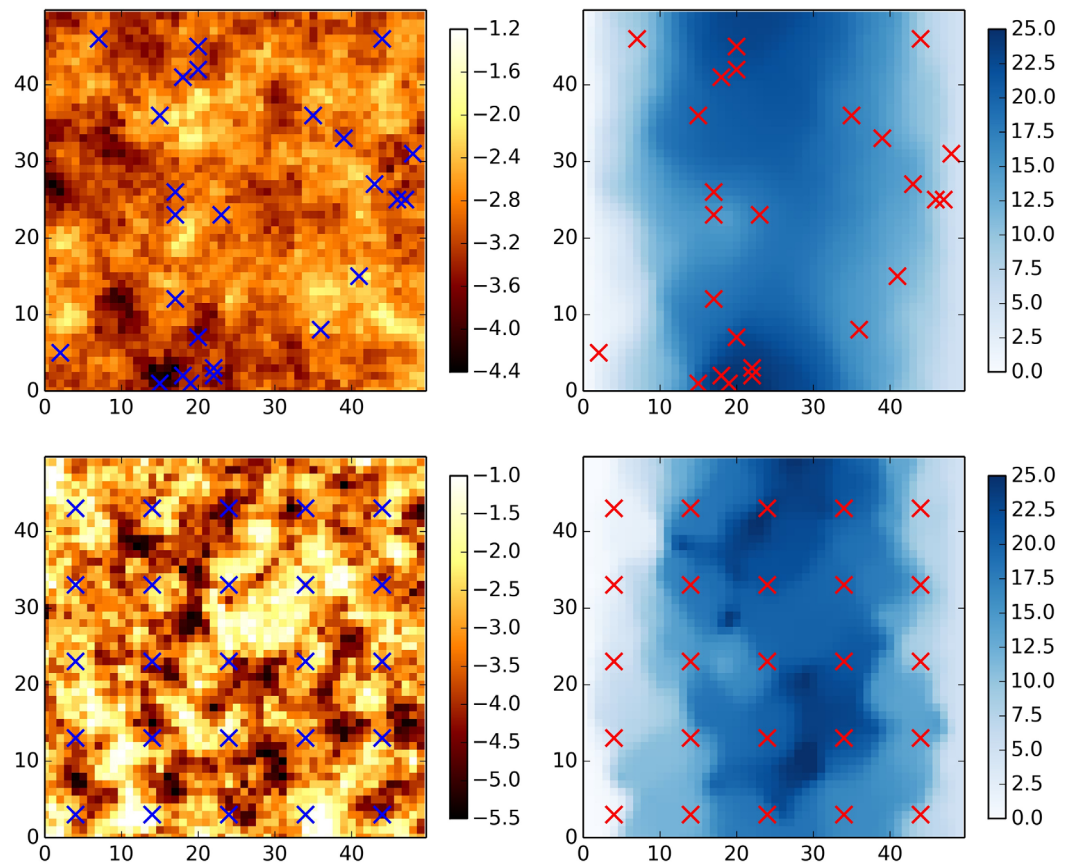
Figure 3. (left) Reference $\log_{10}$ hydraulic transmissivity Y ($\log_{10}(\mathrm{m}^2/\mathrm{s})$) field and (right) corresponding reference hydraulic head h (m) field. Cross denotes the conditioning point locations. The upper fields belong to the mildly heterogeneous test case and the lower fields belong to the strongly heterogeneous test case.

the use of examples that are especially designed to highlight the capabilities of the presented approach and to ensure comparability to other inverse methods, two well-studied synthetic test cases of *Franssen et al.* [2009] are applied to demonstrate the basic methodology. In order to illustrate the possible extensions, one test case is modified.

In both cases, hydraulic transmissivity is considered as an undersampled parameter and its spatial distribution is assumed to be the only unknown of the problem. All other parameters are assumed to be known. Figure 2 shows the general flow setup. The domain length is 4900 m in the x direction and 5000 m in the y direction, discretized into 49 $\times$ 50 grid cells. The northern and southern boundaries share no-flow conditions, while the western and eastern boundaries have prescribed heads of 0 and 5 m, respectively. A pumping well at location (1900 m, 2350 m) pumps steadily with a flow rate of 0.0578 m^3/s and a uniform recharge rate of 362.912 mm/yr is predefined all over the domain.

The first case is mildly heterogeneous; the log transmissivity has a mean $\log_{10}T$ of -2.932 and a $\log_{10}T$ variance of 0.189 $\log_{10}(\mathrm{m}^2/\mathrm{s})$. An exponential variogram without nugget effect and an effective range of 500 m is assumed.

The second case is strongly heterogeneous, with a mean $\log_{10}T$ of -2.932 and a $\log_{10}T$ variance of 1.0 $\log_{10}(\mathrm{m}^2/\mathrm{s})$. A spherical variogram without nugget effect and an effective range of 500 m is assumed.

The reference log transmissivity (Y) fields and the corresponding reference hydraulic head (h) fields are displayed in Figure 3. Those virtual realities are sampled at 25 locations resulting in two sets of conditioning data for each test case.

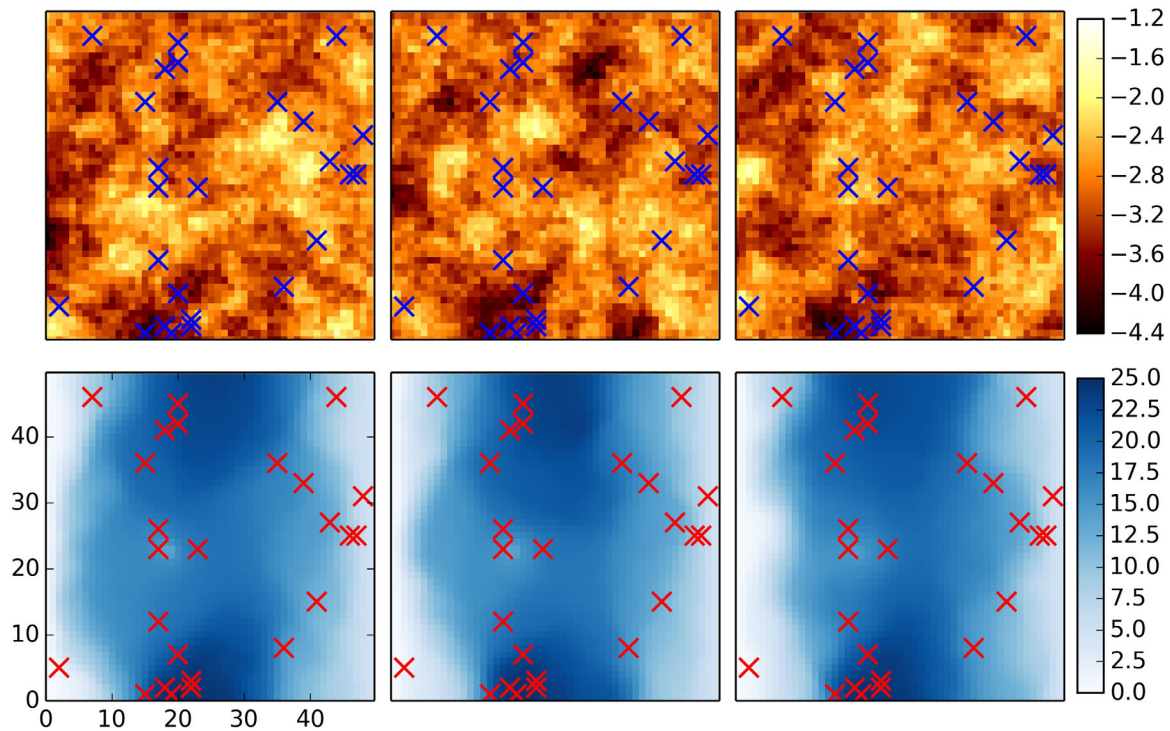According to *Franssen et al.* [2009], the performance of the method is evaluated using three statistics:

Figure 4. (top) Three possible log $_{10}$ transmissivity fields Y (log$_{10}$(m^2/s)) and (bottom) corresponding hydraulic head fields h (m) according to section 5.1.

1. Average absolute error:

$$AAE(X) = \frac{1}{N} \sum_{i=1}^{N} |\overline{X}_i - X_{ref,i}| \tag{28}$$

with N being the number of elements, X the variable of interest, and $\overline{X}$ the mean of the variable of interest over all realizations.

2. Root-mean-square error:

$$RMSE(X) = \sqrt{\frac{1}{N} \sum_{i=1}^{N} \left(\overline{X}_i - X_{ref,i} \right)^2} \tag{29}$$
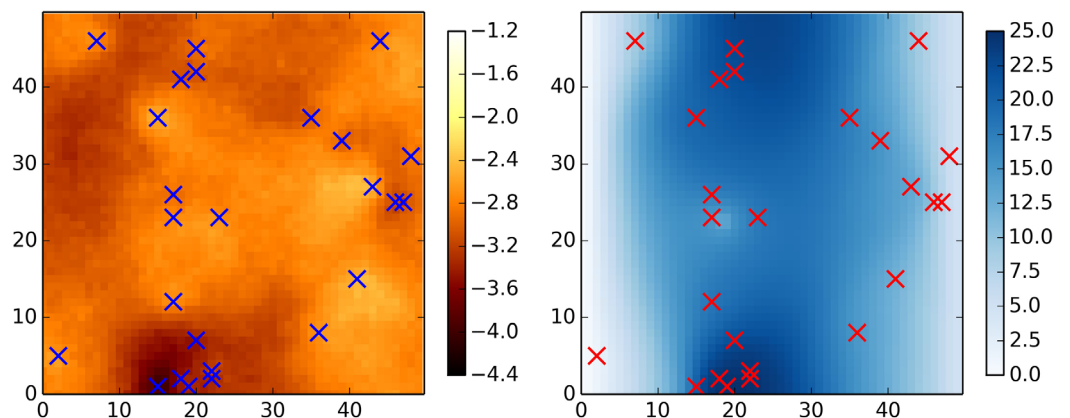
Figure 5. (left) Ensemble mean Y field (log$_{10}$(m^2/s)) and (right) ensemble mean h field (m) over 100 realizations corresponding to section 5.1.
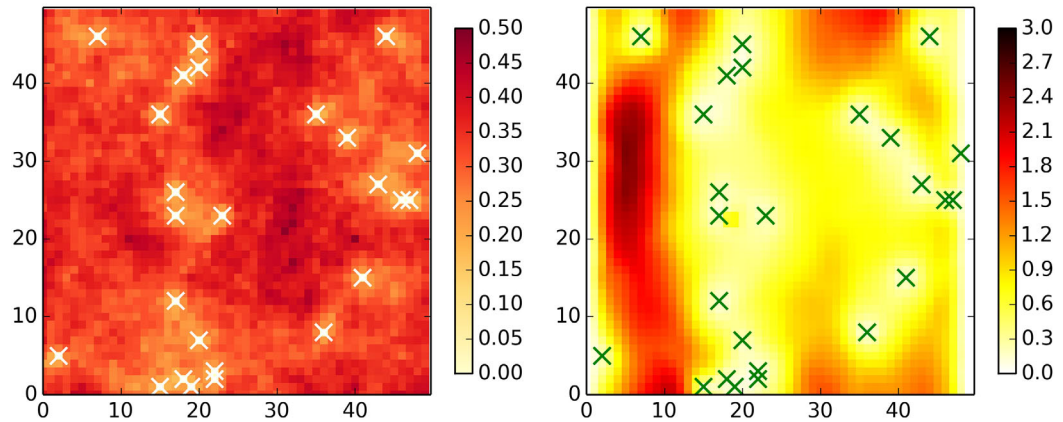
Figure 6. (left) Ensemble Y ($\log_{10}(\mathrm{m^2/s})$) and (right) ensemble h (m) standard deviation corresponding to section 5.1.

Table 1. Performance Statistic Measures for log-T and Hydraulic Head[a]

Example	$AAE(Y)$ ($\log_{10}(\mathrm{m^2/s})$)	$AESD(Y)$ ($\log_{10}(\mathrm{m^2/s})$)	$RMSE(Y)$ ($\log_{10}(\mathrm{m^2/s})$)	$AAE(h)$ (m)	$AESD(h)$ (m)	$RMSE(h)$ (m)
1	0.254	0.331	0.321	0.599	0.808	0.907
4	0.257	0.332	0.323	0.586	0.855	0.899
CY	0.277	0.374	0.348	1.653	2.646	2.151
UNC	0.299	0.437	0.379	1.72	4.25	2.27

[a]1: mildly heterogeneous test case, 4: integral example.

3. Average ensemble standard deviation:

$$AESD(X) = \frac{1}{N}\sum_{i=1}^{N}\sigma_{X_i} \tag{30}$$

with σ_{X_i} being the ensemble standard deviation of variable X at element i.

Besides those comparison measures, standard deviation maps for both Y and h are provided for each example. To illustrate the benefits of the inverse solution, the statistical measures are calculated for two noninverse cases as well. In the first case, the hydraulic transmissivity fields are only conditioned on the spatial model (*UNC*), while in the second case, the transmissivity fields are conditioned on the spatial model as well as on the transmissivity values (*CY*). For both noninverse cases, a stack of 500 simulations is used.

5.1. Basic Case: Lognormal Marginals: Mildly Heterogeneous

The first example represents the mildly heterogeneous test case of *Franssen et al.* [2009]. It is associated with the traditional assumption that the hydraulic transmissivities follow a lognormal spatial distribution. As described in section 2, a normal field is to be identified as $Z(x) = \log W(x)$ with $W(x)$
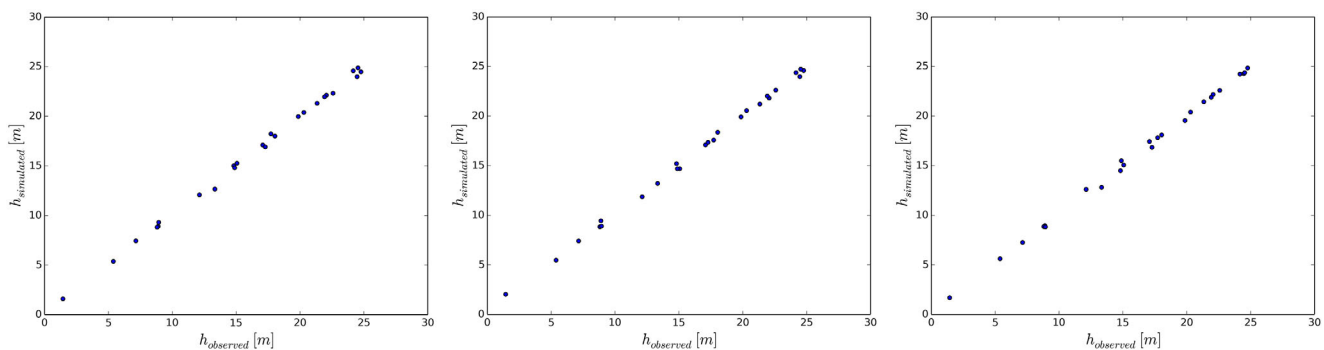

Figure 7. Observed versus simulated hydraulic heads at the observation locations corresponding to section 5.1.
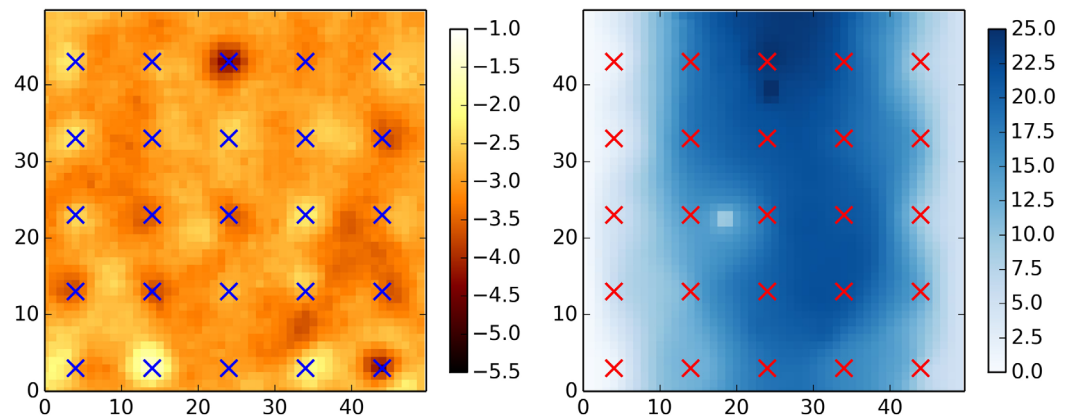
Figure 8. (left) Ensemble mean Y field ($\log_{10}(m^2/s)$) and (right) ensemble mean h field (m) over 100 realizations corresponding to section 5.2.

being the unknown hydraulic transmissivity field. The setup described above is applied, the 25 sampled hydraulic transmissivities are considered as linear equality constraints according to (14). The sampled hydraulic heads are considered as nonlinear constraints according to section 3.3. The objective function measuring the deviation between the simulated head values and the observed head values is

$$\sum_{m=1}^{M} \left(H_{Z_\lambda}(u_m) - h_m \right)^2 \tag{31}$$

and the optimization is terminated if the objective function deceeds a user-defined threshold δ or if the number of iterations (numerical model runs) exceeds a user-defined threshold n_{iter}. Here $\delta = 1\,m^2$ (i.e., a root-mean-squared error of 0.2 m) and $n_{iter} = 1000$.

In total, 100 realizations were generated. Three possible realizations are shown in Figure 4, the ensemble mean fields and the corresponding ensemble standard deviations fields are shown in Figures 5 and 6, respectively. It can be seen that the single realizations of the hydraulic transmissivity fields are allowed to differ among each other while they represent satisfying solutions to the inverse problem. All realizations reproduce the observed transmissivity values exactly and the observed spatial variability is preserved. The provided ensemble mean fields resemble the reference fields, i.e., they are able to reproduce the regions of high and low transmissivity and hydraulic head, respectively. As expected the ensemble standard deviations are lower in regions with higher observation density. The performance measures are displayed in Table 1. The results show that conditioning on transmissivities (CY) already leads to an improved characterization
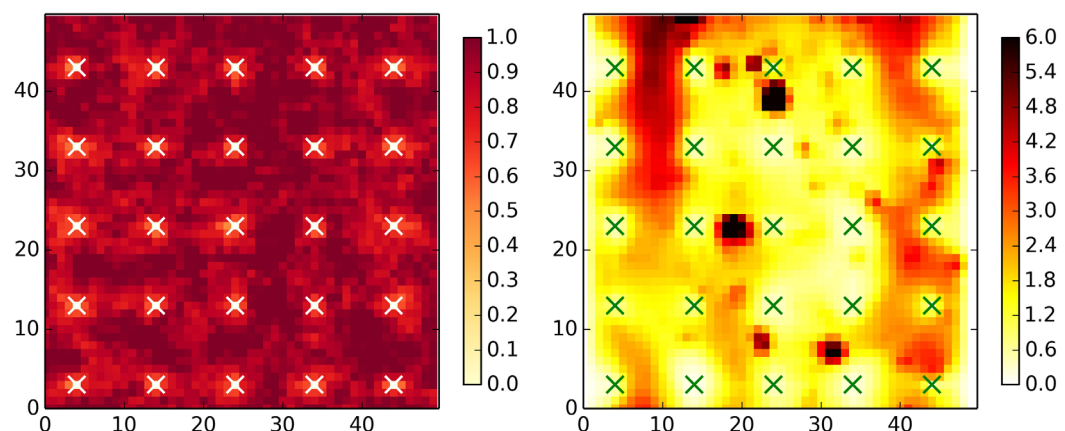

Figure 9. (left) Ensemble Y ($\log_{10}(m^2/s)$) and (right) ensemble h (m) standard deviation corresponding to section 5.2.

Table 2. Performance Statistic Measures for log-T and Hydraulic Head Corresponding To the Strongly Heterogeneous Test Case

Example	$AAE(Y)$ ($\log_{10}(m^2/s)$)	$AESD(Y)$ ($\log_{10}(m^2/s)$)	$RMSE(Y)$ ($\log_{10}(m^2/s)$)	$AAE(h)$ (m)	$AESD(h)$ (m)	$RMSE(h)$ (m)
1	0.712	0.903	0.891	1.182	1.823	1.678
CY	0.741	0.947	0.927	1.896	4.917	2.606
UNC	0.767	0.997	0.954	2.001	5.280	2.725

and to a reduced uncertainty of the transmissivities and the hydraulic heads compared to the unconditional case (*UNC*). Additional conditioning on the observed hydraulic heads triggers further improvements. The average absolute error $AAE(Y)$ of the transmissivities show a reduction of 15.1%. Similar results are found for $RMSE(Y)$. The characterization of the hydraulic head field measured by $AAE(h)$ could be improved by 65%; $RMSE(h)$ shows a reduction of 60%. The uncertainty associated with the transmissivity field, measured by $AESD(Y)$ shows a reduction of 24%. $AESD(h)$ shows a reduction of 81%. Figure 7 shows three scatter plots of observed versus simulated hydraulic heads. It can be seen that not only the average values but also the single values match reasonably. As the performance measures range between those obtained in *Franssen et al.* [2009], it can be concluded that the suggest approach performs in a satisfactory manner regarding the mildly heterogeneous test case.

5.2. Basic Case: Lognormal Marginals: Strongly Heterogeneous

The second example represents the strongly heterogeneous test case of *Franssen et al.* [2009]. The hydraulic transmissivities are again assumed to follow a lognormal spatial distribution but with a higher $\log_{10}T$ variance compared to the first case. Again the general flow setup as described in section 5 is applied. As in the first example, the 25 sampled hydraulic transmissivities are considered as linear equality constraints according to (14), the sampled hydraulic heads are considered as nonlinear constraints according to section 3.3. The objective function is again (31) and 100 realizations are generated. Here $\delta = 2\,m^2$ (i.e., a root-mean-squared error of 0.28 m) and the threshold number of iterations is $n_{iter} = 3000$.

Figure 8 shows the resulting ensemble mean fields, Figure 9 shows the ensemble standard deviation fields. The performance measures are displayed in Table 2. As expected, the improvements are smaller than in the mildly heterogeneous test case. This is however a common observation in inverse modeling studies.
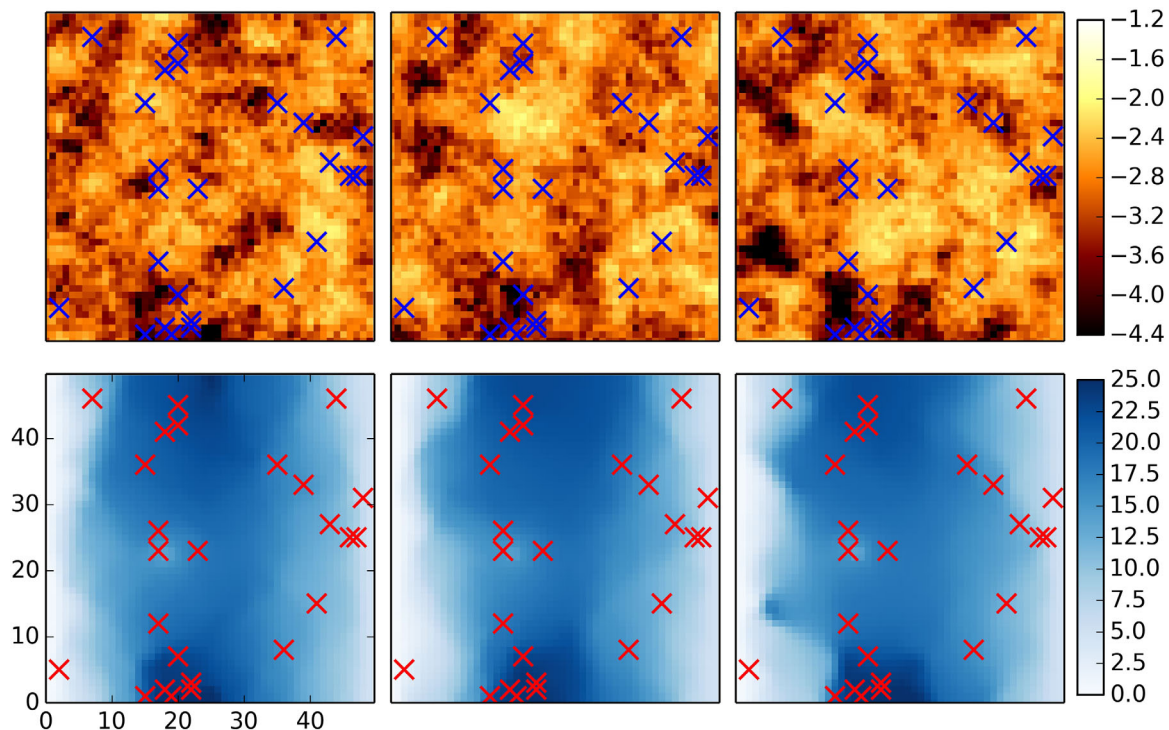

Figure 10. (top) Three possible $\log_{10}$ transmissivity fields Y ($\log_{10}(m^2/s)$) and (bottom) corresponding hydraulic head fields h (m) according to section 5.3.
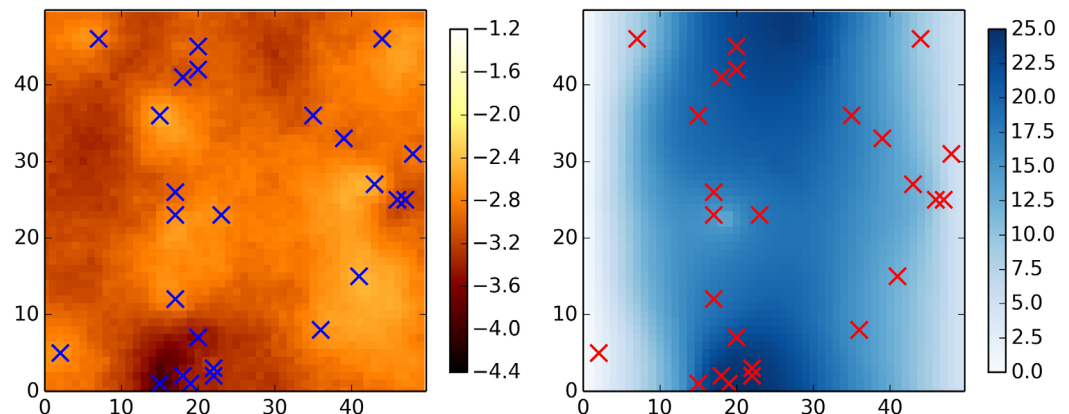
Figure 11. (left) Ensemble mean Y field ($\log_{10}(\mathrm{m}^2/\mathrm{s})$) and (right) ensemble mean h field (m) over 100 realizations corresponding to section 5.3.

Conditioning on the observed transmissivities (CY) reduces $AAE(Y)$ by only 3.4% while the inverse solution shows a reduction of 7.1%. Similar results are obtained for $RMSE(Y)$ and $AESD(Y)$. In general, larger heterogeneity is more demanding. Thus, the optimization process is more difficult and less effective. However, the results are again reasonable as the performance measures range between those obtained in *Franssen et al.* [2009].

5.3. Non-Lognormal Marginal

The third example requires a slight modification of the mildly heterogeneous test case. The assumption that the hydraulic transmissivities follow a lognormal distribution is relaxed toward an arbitrary marginal distribution with a Gaussian copula dependence structure. Here it is assumed that the transmissivities follow an exponential distribution. On that account, an exponential distribution $F(w) = 1 - e^{-\lambda w}$ is fitted to the 25 sampled transmissivity values. As described in section 3.1, the hydraulic transmissivity field $W(x)$ can be transformed to a multinormal field $Z(x)$ according to (9). Thus, it is assumed that the spatial dependence structure is multivariate Gaussian while the marginal distribution is exponential. Besides those changes, the general setup remains as described in section 5.1. The transmissivity values are again treated as linear constraints according to (14), the hydraulic head values as nonlinear constraints according to section 3.3. The objective function is (31) and 100 realizations are generated.

Three possible hydraulic transmissivity fields with corresponding hydraulic head fields are displayed in Figure 10. The corresponding mean fields, as well as the standard deviation fields, are shown in Figures 11 and 12, respectively. It can be seen that due to the influence of the different marginal distribution, the Y fields as well as the h fields differ slightly from those obtained in section 5.1. However, the mean fields still
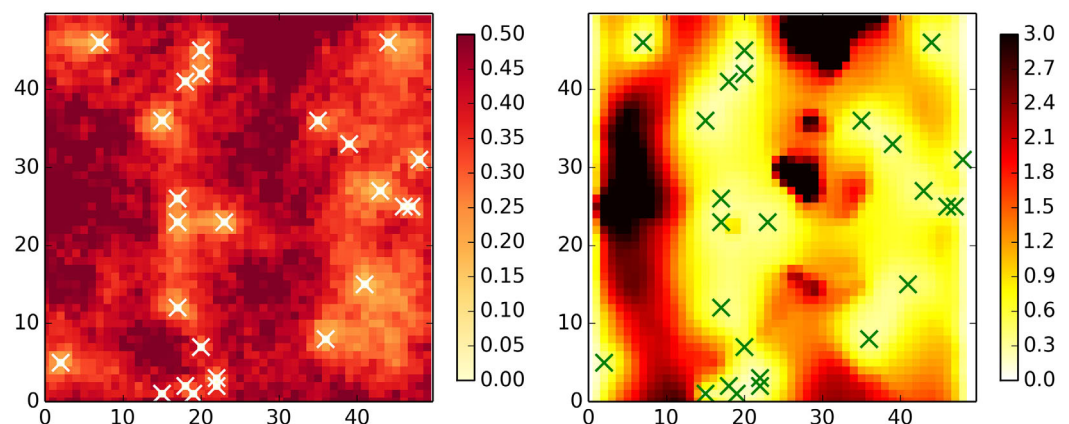

Figure 12. (left) Ensemble Y ($\log_{10}(\mathrm{m}^2/\mathrm{s})$) and (right) ensemble h (m) standard deviation corresponding to section 5.3.
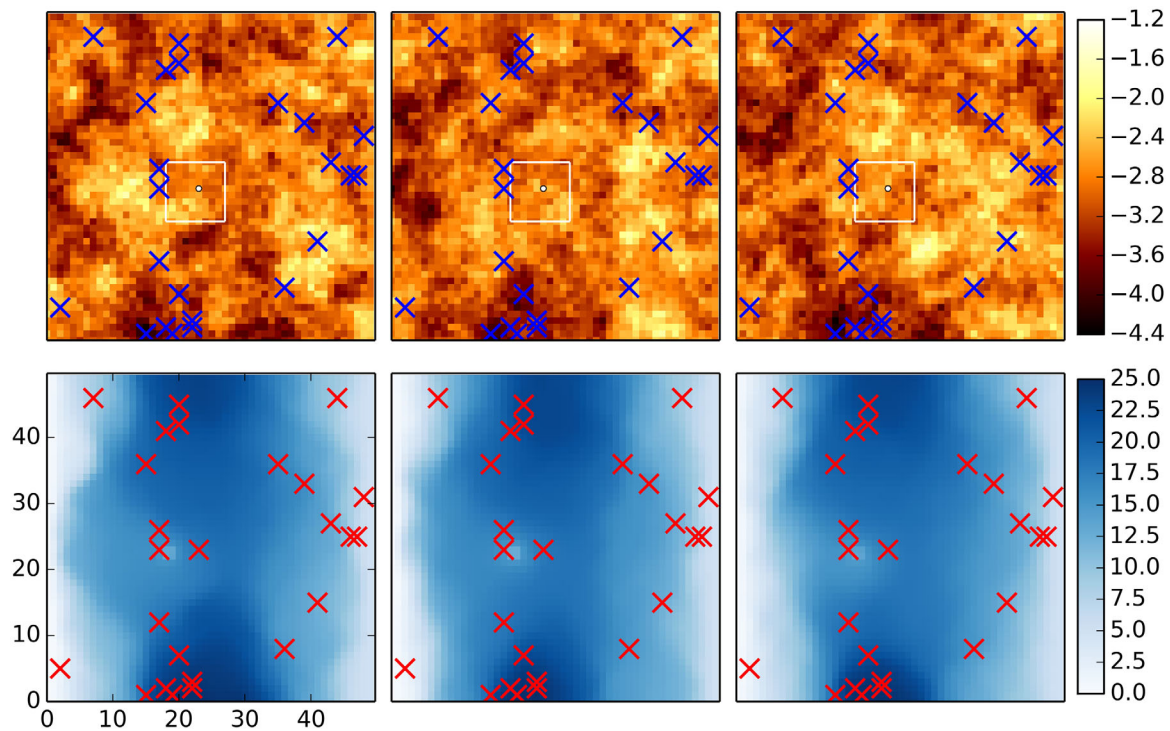
Figure 13. (top) Three possible $\log_{10}$ transmissivity fields Y ($\log_{10}(m^2/s)$) and (bottom) corresponding hydraulic head fields h (m) according to section 5.4.

resemble the reference ones reasonably, i.e., they are able to reflect zones of high and low transmissivity and hydraulic head, respectively. The exponential marginal distribution leads to a higher variance of the transmissivity fields compared to the basic mildly heterogeneous case. Thus, the standard deviations are also slightly higher than those obtained in section 5.1.

A comparison of the performance measures would be futile as this example and the reference case are based on different assumptions. However, it is worth pointing out that satisfactory solutions to the inverse problem can be achieved even though different assumptions are considered.

5.4. Change of Support: Integral Constraints

This example is associated with the problem of scales of inverse methods. There are different spatial scales at which information is commonly handled in inverse groundwater modeling. For example, measurements from boreholes represent punctual values while local pumping tests result in average values that are valid
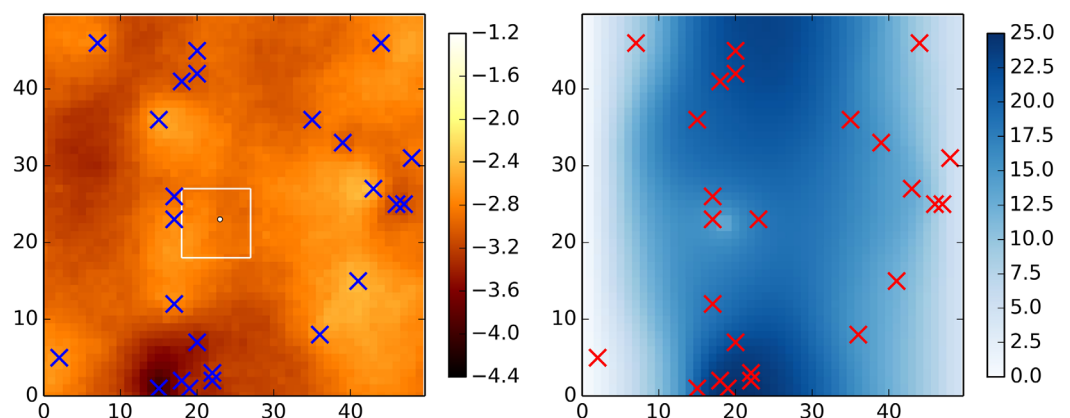

Figure 14. (left) Ensemble mean Y field ($\log_{10}(m^2/s)$) and (right) ensemble mean h field (m) over 100 realizations corresponding to section 5.4.
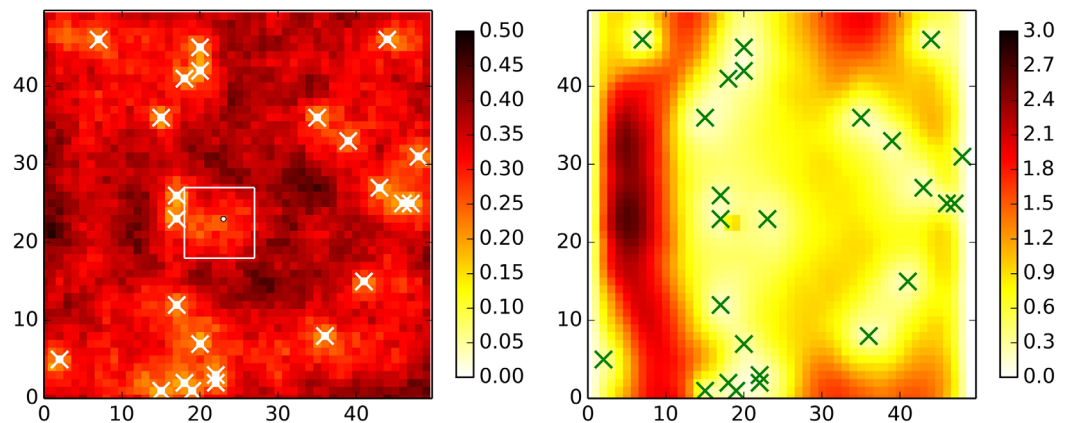
Figure 15. (left) Ensemble Y ($\log_{10}(\text{m}^2/\text{s})$) and (right) ensemble h (m) standard deviation corresponding to section 5.4.

on a larger scale [*Schad and Teutsch*, 1994]. Taking information on different spatial scales into one model is a frequent and challenging task in inverse groundwater modeling [*Zhou et al.*, 2014].

This example demonstrates how integral constraints can be taken into account as additional nonlinear constraints. Therefore, the mildly heterogeneous case is considered where one of the 25 measured hydraulic transmissivities is replaced by an integral value. The integral is rectangular with a size of 10×10 pixels surrounding the actual (replaced) conditioning point. Its values are the geometrical mean of the values obtained from the reference field. As the integral is an additional nonlinear constraint, the objective function which has to be minimized is changed to $f_{obj} = \sum_{m=1}^{M} (H_{Z_\lambda}(u_m) - h_m)^2 + I$ with $I = 0$ if the deviation of simulated and observed integral value is less than 5% else $I = 666$.

Again 100 realizations are generated and three resulting hydraulic transmissivity fields with corresponding hydraulic head fields are shown in Figure 13. The performance measures are listed in Table 1. From Figure 14, it can be seen that the reference fields could be resembled reasonably. Figure 15 shows the ensemble
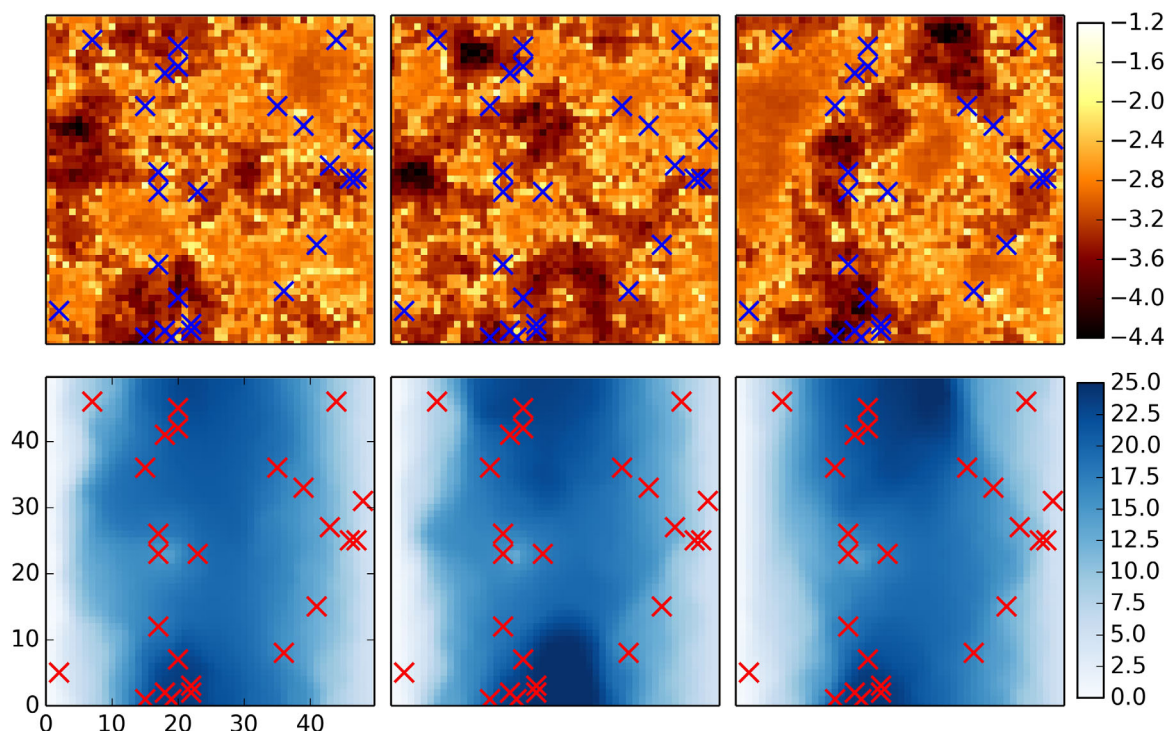

Figure 16. (top) Three possible $\log_{10}$ transmissivity fields Y ($\log_{10}(\text{m}^2/\text{s})$) and (bottom) corresponding hydraulic head fields h (m) according to section 5.5.
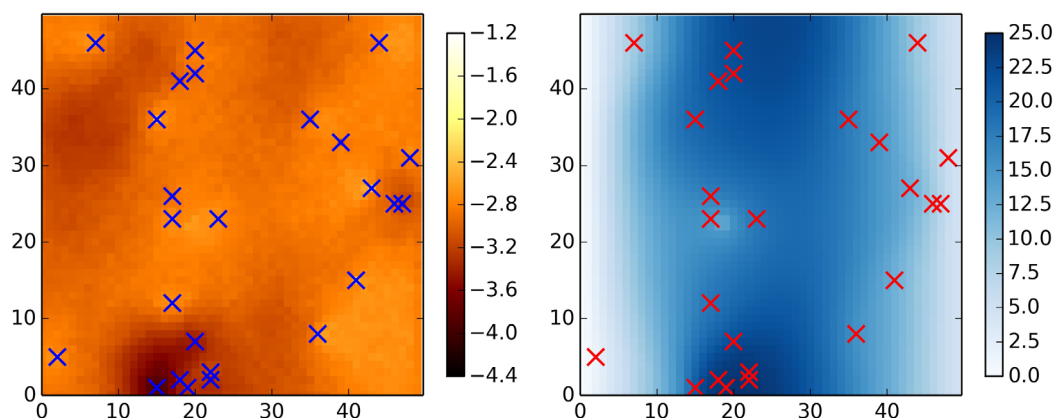
Figure 17. (left) Ensemble mean Y field ($\log_{10}(\mathrm{m^2/s})$) and (right) ensemble mean h field (m) over 200 realizations corresponding to section 5.5.

standard deviation fields. It is worth noting that the standard deviation inside the integral is not zero as only the mean value has to be matched (with a tolerance of 5%). However, the standard deviation inside the integral is much lower than in the surrounding.

5.5. Non-Gaussian Spatial Structures

As described in section 3.4, the spatial dependence structure of hydraulic transmissivities might differ significantly from Gaussian. Such non-Gaussian spatial dependence structures might have substantial influence on flow and transport processes. This example aims to take such asymmetrical dependence structures into account: for that reason, the synthetic mildly heterogeneous test case is again modified. The spatial dependence structure of the hydraulic transmissivities is no longer assumed to be multivariate Gaussian; instead, a v-transformed normal copula, as presented in *Bárdossy and Li* [2008], is used to model the dependence structure. v-Copulas are able to describe asymmetrical dependence structures, i.e., high values can cluster differently than low values. A v-copula is fitted to the 25 hydraulic transmissivity values and the inverse modeling approach is changed according to section 3.4. Aside from the modification described above, the setup remains as described in section 5.1. Thus, the spatial dependence structure of the hydraulic transmissivities is assumed to be non-Gaussian while the marginal distribution remains lognormal.

To achieve a stable mean, 200 realizations are generated. Figure 16 shows three hydraulic transmissivity fields with corresponding hydraulic head fields. It can be seen that the spatial dependence structure clearly exhibits a non-Gaussian behavior. The low values as well as values around the mean form
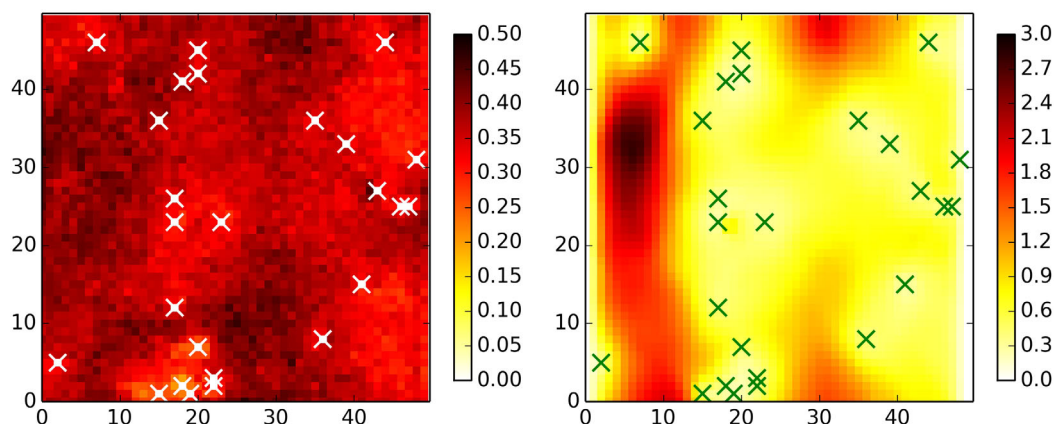

Figure 18. (left) Ensemble Y ($\log_{10}(\mathrm{m^2/s})$) and (right) ensemble h (m) standard deviation corresponding to section 5.5.
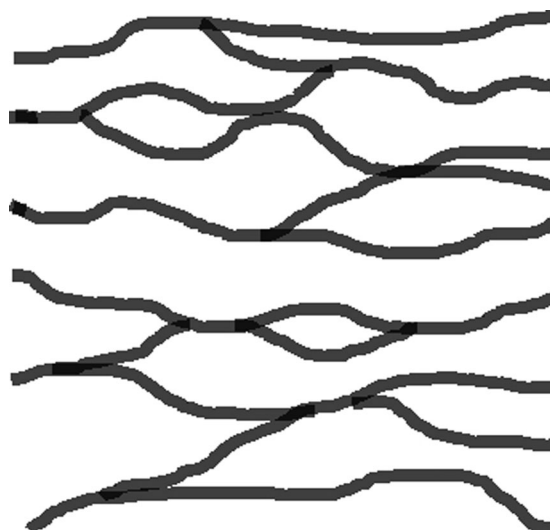
Figure 19. Training image representing the two-facies geological formation corresponding to section 5.6.

connected clusters, while high values occur occasionally, or form somehow connected flow paths. However, the observed transmissivity values are represented exactly and the corresponding hydraulic head fields are reasonable. Figure 17 shows the ensemble mean fields which are capable of identifying the zones of low and high transmissivity and hydraulic head, respectively. Figure 18 shows the ensemble standard deviation fields. As a result of the assumed non-Gaussian spatial structure the standard deviations are higher compared to the basic Gaussian case. However, the coarse patterns are similar.

As in section 5.3, a comparison of the performance measures would be meaningless as different assumptions are considered. However, this example shows that non-Gaussian spatial dependence structures can be considered using non-Gaussian spatial copulas. Even though the resulting transmissivity fields clearly exhibit different spatial patterns of variability compared to the basic test case, they represent satisfying solutions to the actual inverse problem.

5.6. Including Known Geological Structure Information

As described in section 3.5, it is often assumed that geological processes lead to hydraulic transmissivities that are structured in a specific way. Including such curvilinear features in the spatial distribution of the transmissivities goes beyond the traditional Gaussian assumption (second-order moment statistics) and induces the necessity to account for higher-order moments. One possibility of considering such spatial structures is to use multiple-point geostatistics [*Strebelle*, 2002]. According to section 3.5, the presented random mixing approach can be coupled with a multiple-point approach, so that structural information obtained from a training image can be incorporated in the inverse modeling procedure. Hence, the large-scale structure (macrostructure) results from multiple-point geostatistics while the small-scale structure (microstructure) is modeled by random mixing.

To illustrate this coupled approach, a new synthetic example is generated. The domain length is 5000 m in x and y direction, discretized in 50×50 grid cells. The northern and southern boundaries share no-flow conditions. The western and eastern boundaries have prescribed heads of 20 and 1 m, respectively. A two-facies geological formation is considered. Each facies has its own marginal distribution: facies A (connected
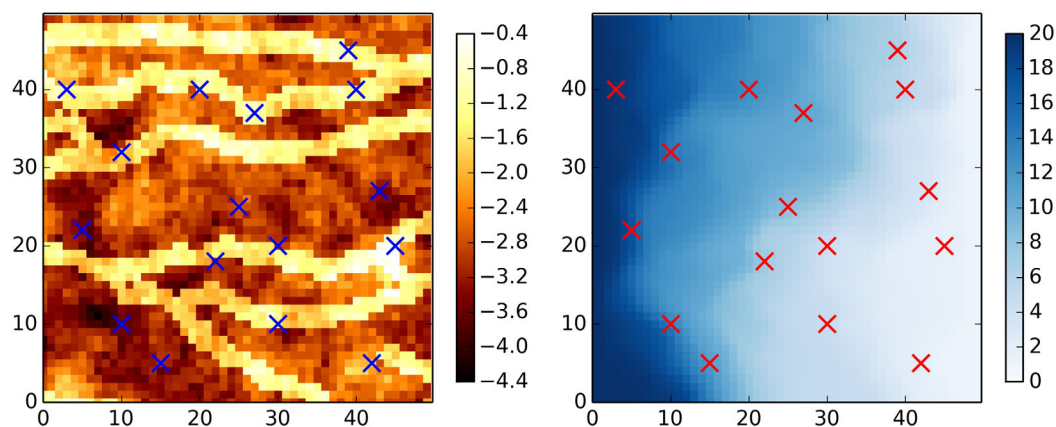

Figure 20. (left) Reference log$_{10}$ hydraulic transmissivity field Y ($\log_{10}(m^2/s)$) and (right) corresponding hydraulic head h (m) field corresponding to section 5.6.
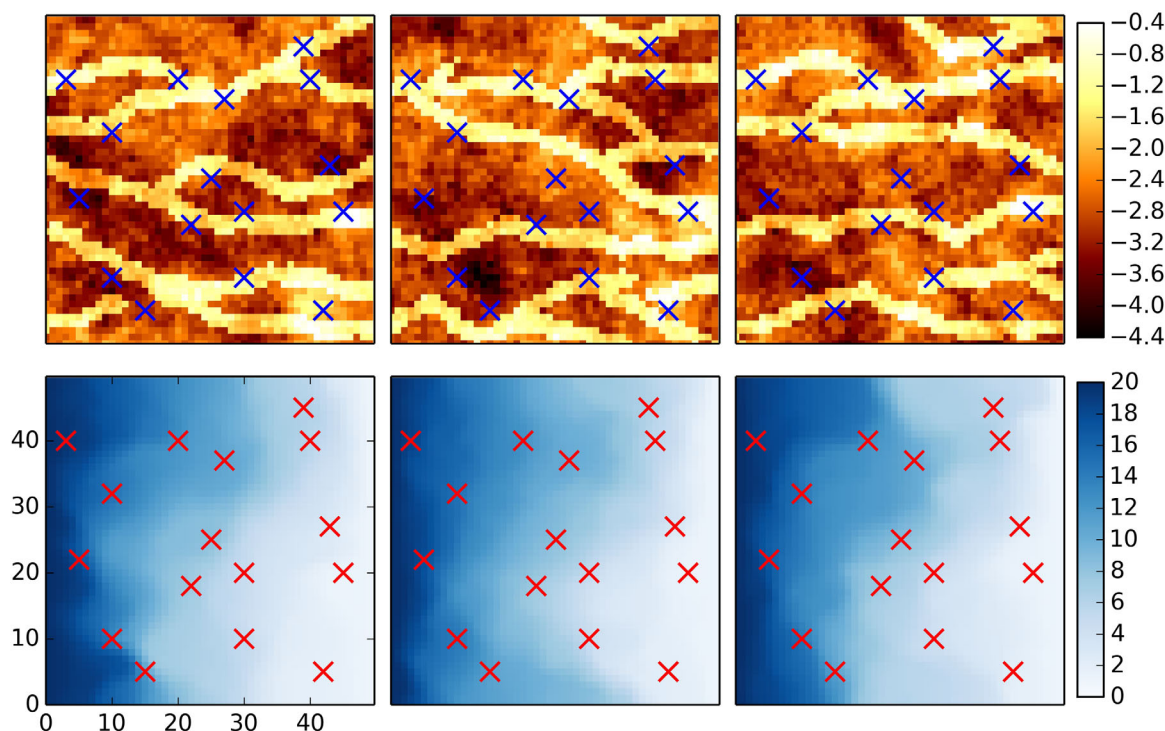
Figure 21. (top) Three possible log $_{10}$ hydraulic transmissivity fields (log$_{10}$(m^2/s)) and (bottom) corresponding hydraulic head fields h (m) according to section 5.6.

flow paths) exhibits a lognormal distribution with a mean log $_{10}T$ of -1.5 and a log $_{10}T$ variance equal to 0.189, while facies B exhibits a lognormal distribution sharing the same variance but a mean log $_{10}T$ of -2.932. A direct sampling algorithm *Mariethoz et al.* [2010] is applied to generate conditional realizations of the training image (Figure 19) which represents the assumed two-facies formation. A Gaussian copula is used to model the small-scale dependence structure inside each facies. The reference Y and h fields are shown in Figure 20. Those are sampled at 16 locations resulting in three sets of conditioning data: one set on the geological structure information, one set on the actual hydraulic transmissivity values, and one set on the corresponding hydraulic head values. The inverse modeling approach is changed according to section 3.5. The objective function measuring the mismatch between simulated hydraulic head and observed hydraulic head is (31). In total, 200 realizations were generated. Three possible solutions are shown in Figure 21. The large-scale structure, as well as the small-scale structure, differs strongly among the different realizations while the conditions on the geological structure (to which facies the value belongs) and the corresponding hydraulic transmissivity values are exactly fulfilled. Figure 22 shows the ensemble mean fields,
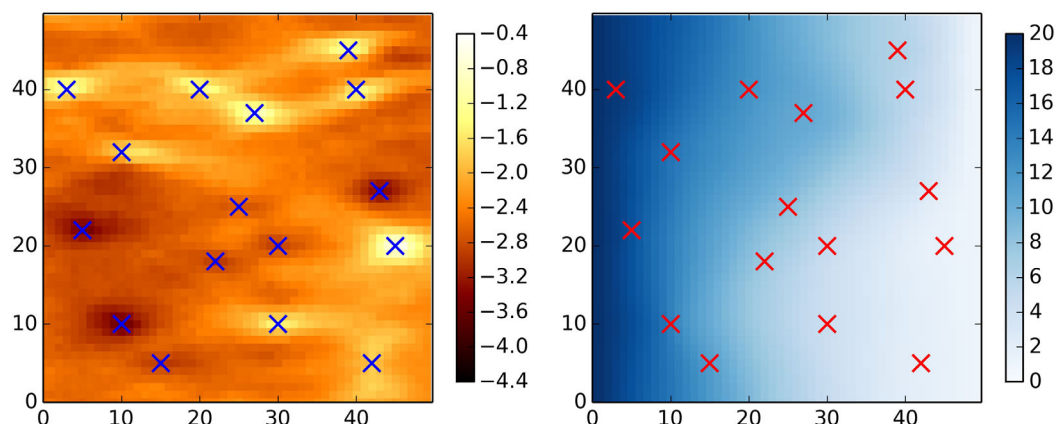

Figure 22. Ensemble mean Y field and ensemble mean h field over 200 realizations corresponding to section 5.6.
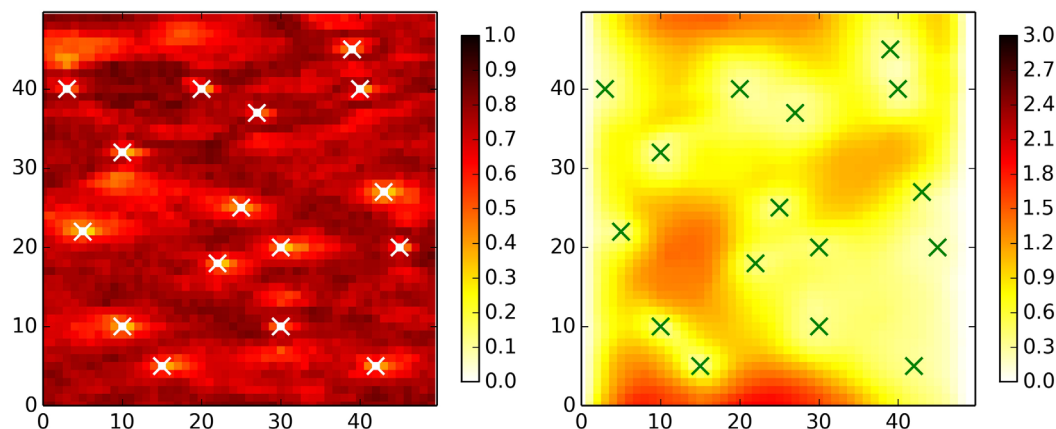
Figure 23. Ensemble Y ($\log_{10}(\text{m}^2/\text{s})$) and h (m) standard deviation corresponding to section 5.6.

Figure 23 shows the ensemble standard deviation fields. The mean hydraulic head field reproduces the reference one reasonably well. The average hydraulic transmissivity field resembles zones of high and low transmissivity, respectively. Even though it is not optimized during the calibration process, the average transmissivity field reflects the macrostructure to some extent. Especially, in the upper part of the transmissivity field. Nevertheless, a coupled optimization of the macrostructure and microstructure could lead to better results.

6. Discussion and Conclusion

In this paper, a new Monte Carlo based methodology to generate random hydraulic transmissivity fields that are solutions of the inverse groundwater flow problem was presented. The methodology is based on spatial copulas and allows arbitrary marginal distributions. The solutions are obtained as a linear combination of unconditional realizations of the fields, where the weights are identified on an appropriate subspace via unconstrained optimization.

The advantages of the method are as follows:

1. High flexibility to cope with different spatial dependence structures and arbitrary marginal distributions.
2. Continuous and unconstrained formulation of the nonlinear constraints, which relate the hydraulic transmissivity fields to the observed hydraulic heads.
3. Combination with multiple-point statistics to integrate prescribed structural information.

The general applicability of random mixing to inverse groundwater modeling is first demonstrated using the two examples. Those examples have been investigated in other studies using different inverse modeling approaches. Thus, the results can easily be compared to each other. The first example is a mildly heterogeneous test case while the second example is strongly heterogeneous. If compared to the outcomes of other studies, the results obtained using random mixing are satisfactory in both test cases. The statistical performance measures range between those obtained by other methods. Note however that the goal of this paper was not to produce "better" or computationally "cheaper" results for the two test cases. The focus is more on the flexible extensions of the basic approach, i.e., non-Gaussian marginals, non-Gaussian spatial dependence structures, and integral constraints. Those extensions are demonstrated using the remaining examples.

The third example uses a Gaussian copula to describe the spatial dependence structure of the hydraulic transmissivities while the marginal follows an exponential distribution. Hence, the spatial dependence is multivariate Gaussian with a non-Gaussian marginal distribution. This example demonstrates how the suggested approach can be applied to solve the inverse problem if the observed transmissivities do not follow a lognormal marginal distribution while the spatial dependence is Gaussian. A main conclusion that can be drawn from this example is that even though a different marginal distribution is assumed one can still achieve satisfactory solutions to the given inverse problem. This however leads to an increased overall uncertainty as both the lognormal as well as the exponential distribution can be applied to solve the problem.

The fourth example demonstrates how information on different spatial scales can be handled. It is shown that arbitrary integral constraints can be incorporated as additional nonlinear constraints.

The fifth example demonstrates how certain non-Gaussian spatial dependence structures can be handled. This approach has the significant advantage compared to other non-Gaussian inverse modeling techniques that no training image is required. Instead, the parameters of the non-Gaussian copula used to model the spatial dependence are estimated from the observed data directly. Thus, no assumptions on a possible training image have to be made. An interesting result of this example is that the single realizations clearly exhibit non-Gaussian spatial dependence structures, whereas the ensemble average transmissivity field resembles the reference field reasonably well. This leads to an increased overall uncertainty as not only the spatial model parameters but even its structure (copula model) has to be considered as uncertain. Additional diagnostic tools are required to reduce the uncertainty of the identification of the spatial structures, and their parameter estimation.

The suggested approach can be coupled to multiple-point statistics as presented in the sixth example. The difference to other methods using multiple-point statistics is that here the macrostructure and microstructure of the transmissivity field are modeled separately. While the macrostructure, which represents a facies distribution is modeled using a multipoint approach, the microstructure is modeled using random mixing. The results obtained are promising, nevertheless this approach has to be improved as the macrostructure is not changed during the optimization process. A coupled treatment, where the likelihood of the multipoint realization is assessed in combination with the microstructure during the optimization would probably lead to a better representation of the combined uncertainty.

The copula-based approach uses parametric models for the description of spatial variability. The conditions for a copula family to be used as a spatial model [*Bárdossy*, 2006] are restrictive, thus it is difficult to find suitable models. Models described in *Bárdossy and Li* [2008] provide examples for the simulation of a wide range of spatial patterns, but unfortunately parameter inference problems for many of these models are not solved yet. Further the consideration of conditioning observations can become computationally very time consuming. For this paper, a specific family of copulas, which could be derived via noninvertible transformations of the normal, were used. These can account for asymmetrical properties of observations which characterize certain natural processes on small and medium scales. Efficient modeling of large-scale features using copulas requires further research.

In general, the suggested approach gives promising results and represents a reasonable alternative or extension to training image based non-Gaussian inverse modeling. As the method is very general, it is not limited to inverse groundwater flow modeling. More complex cases like flow and transport modeling can also be treated. 3-D problems can also be handled with only slight modifications of the methodology. However, as is common in Monte Carlo based approaches, the limiting factor of large-scale applications is the complexity of the numerical model.

References

Alcolea, A., and P. Renard (2010), Blocking moving window algorithm: Conditioning multiple-point simulations to hydrogeological data, *Water Resour. Res.*, *46*, W08511, doi:10.1029/2009WR007943.

Arpat, G. B., and J. Caers (2007), Conditional simulation with patterns, *Math. Geol.*, *39*(2), 177–203, doi:10.1007/s11004-006-9075-3.

Bárdossy, A. (2006), Copula-based geostatistical models for groundwater quality parameters, *Water Resour. Res.*, *42*, W11416, doi:10.1029/2005WR004754.

Bárdossy, A., and J. Li (2008), Geostatistical interpolation using copulas, *Water Resour. Res.*, *44*, W07412, doi:10.1029/2007WR006115.

Caers, J. (2003), Efficient gradual deformation using a streamline-based proxy method, *J. Pet. Sci. Eng.*, *39*, 57–83.

Caers, J., and T. Hoffman (2006), The probability perturbation method: A new look at Bayesian inverse modeling, *Math. Geol.*, *38*(1), 81–100, doi:10.1007/s11004-005-9005-9.

Dietrich, C., and G. Newsam (1996), A fast and exact method for multidimensional Gaussian stochastic simulations: Extension to realizations conditioned on direct and indirect measurements, *Water Resour. Res.*, *32*(6), 1643–1652.

Evensen, G. (2003), The ensemble Kalman filter: Theoretical formulation and practical implementation, *Ocean Dyn.*, *53*(4), 343–367, doi:10.1007/s10236-003-0036-9.

Franssen, H., A. Alcolea, M. Riva, M. Bakr, N. van der Wiel, F. Stauffer, and A. Guadagnini (2009), A comparison of seven methods for the inverse modelling of groundwater flow. Application to the characterisation of well catchments, *Adv. Water Resour.*, *32*, 851–872.

Franssen, H.-J. H., J. Gómez-Hernández, and A. Sahuquillo (2003), Coupled inverse modelling of groundwater flow and mass transport and the worth of concentration data, *J. Hydrol.*, *281*(4), 281–295, doi:10.1016/S0022-1694(03)00191-4.

Freeze, A. R. (1975), A stochastic-conceptual analysis of one-dimensional groundwater flow in nonuniform homogeneous media, *Water Resour. Res.*, *11*(5), 725–741.

Fu, J., and J. J. Gómez-Hernández (2008), A blocking Markov chain Monte Carlo method for inverse stochastic hydrogeological modeling, *Math. Geosci.*, *41*(2), 105–128, doi:10.1007/s11004-008-9206-0.

Golub, G., and W. Kahan (1965), Calculating the singular values and pseudo-inverse of a matrix, *J. Soc. Ind. Appl. Math.*, *2*(2), 205–224.

Gómez-Hernández, J. J., and X. Wen (1998), To be or not to be multi-Gaussian? A reflection on stochastic hydrogeology, *Adv. Water Resour.*, *21*(1), 47–61.

Gómez-Hernández, J. J., A. Sahuquillo, and J. E. Capilla (1997), Stochastic simulation of transmissivity fields conditional to both transmissivity and piezometric data—I. Theory, *J. Hydrol.*, *203*(14), 162–174, doi:10.1016/S0022-1694(97)00098-X.

Guardiano, F., and R. Srivastava (1993), Multivariate geostatistics: Beyond bivariate moments, in *Geostatistics Tria 92, Quantitative Geology and Geostatistics*, vol. 5, edited by A. Soares, pp. 133–144, Springer, Netherlands, Dordrecht, doi:10.1007/978-94-011-1739-5\12.

Guthke, P. (2013), *Non-Multi Gaussian Spatial Structures: Process-Driven Natural Genesis, Manifestation, Modeling Approaches, and Influences on Dependent Processes*, Eigenverlag Inst. Wasserbau, Stuttgart.

Guthke, P., and A. Bárdossy (2012), Reducing the number of {MC} runs with antithetic and common random fields, *Adv. Water Resour.*, *43*, 1–13, doi:10.1016/j.advwatres.2012.03.014.

Haslauer, C., P. Guthke, A. Bárdossy, and E. Sudicky (2012), Effects of non-Gaussian copula-based hydraulic conductivity fields on macrodispersion, *Water Resour. Res.*, *48*, W07507, doi:10.1029/2011WR011425.

Hastings, W. K. (1970), Monte Carlo sampling methods using Markov chains and their applications, *Biometrika*, *57*(1), 97–109.

Hendricks Franssen, H. J., and W. Kinzelbach (2008), Real-time groundwater flow modeling with the ensemble Kalman filter: Joint estimation of states and parameters and the filter inbreeding problem, *Water Resour. Res.*, *44*, W09408, doi:10.1029/2007WR006505.

Hu, L. (2000), Gradual deformation and iterative calibration of Gaussian-related stochastic models, *Math. Geol.*, *32*(1), 87–108.

Hu, L., Y. Zhao, Y. Liu, C. Scheepens, and A. Bouchard (2013), Updating multipoint simulations using the ensemble Kalman filter, *Comput. Geosci.*, *51*, 7–15.

Hu, L. Y. (2002), Combination of dependent realizations within the gradual deformation method, *Math. Geol.*, *34*(8), 953–963.

Hu, L. Y., G. Blanc, and B. Noetinger (2001), Gradual deformation and iterative calibration of sequential stochastic simulations, *Math. Geol.*, *33*(4), 475–489.

Huysmans, M., and A. Dassargues (2010), Application of multiple-point geostatistics on modelling groundwater flow and transport in a cross-bedded aquifer, in *geoENV VII Geostatistics for Environmental Applications, Quantitative Geology and Geostatistics*, vol. 16, edited by P. M. Atkinson and C. D. Lloyd, pp. 139–150, Springer, Netherlands, doi:10.1007/978-90-481-2322-3\13.

Jafarpour, B., and M. Khodabakhshi (2011), A probability conditioning method (PCM) for nonlinear flow data integration into multipoint statistical facies simulation, *Math. Geosci.*, *43*, 133–164.

Journel, A., and T. Zhang (2006), The necessity of a multiple-point prior model, *Math. Geol.*, *38*(5), 591–610, doi:10.1007/s11004-006-9031-2.

Journel, A. G. (1974), Geostatistics for conditional simulation of ore bodies, *Econ. Geol. Bull. Soc. Econ. Geologists*, *69*(5), 673–687.

Li, L., H. Zhou, H. H. Franssen, and J. Gómez-Hernández (2012), Groundwater flow inverse modeling in non-multiGaussian media: Performance assessment of the normal-score ensemble Kalman filter, *Hydrol. Earth Syst. Sci.*, *16*(2), 573–590.

Mariethoz, G., P. Renard, and J. Straubhaar (2010), The Direct Sampling method to perform multiple-point geostatistical simulations, *Water Resour. Res.*, *46*, W11536, doi:10.1029/2008WR007621.

Michalak, A. M. (2008), A Gibbs sampler for inequality-constrained geostatistical interpolation and inverse modeling, *Water Resour. Res.*, *44*, W09437, doi:10.1029/2007WR006645.

Nelson, R. (1999), *An Introduction to Copulas*, Springer, N. Y.

Oliver, D. S., L. B. Cunha, and A. C. Reynolds (1997), Markov chain Monte Carlo methods for conditioning a permeability field to pressure data, *Math. Geol.*, *29*(1), 61–91.

Pérez, C., G. Mariethoz, and J. M. Ortiz (2014), Verifying the high-order consistency of training images with data for multiple-point geostatistics, *Comput. Geosci.*, *70*, 190–205, doi:10.1016/j.cageo.2014.06.001.

Powell, M. J. D. (1998), Direct search algorithms for optimization calculations, *Acta Numer.*, *7*, 287–336, doi:10.1017/S0962492900002841.

RamaRao, B. S., A. M. LaVenue, G. De Marsily, and M. G. Marietta (1995), Pilot point methodology for automated calibration of an ensemble of conditionally simulated transmissivity fields: 1. Theory and computational experiments, *Water Resour. Res.*, *31*(3), 475–493.

Riva, M., S. Neuman, and A. Guadagnini (2013), Sub-Gaussian model of processes with heavy-tailed distributions applied to air permeabilities of fractured tuff, *Stochastic Environ. Res. Risk Assess.*, *27*(1), 195–207.

Ronayne, M. J., S. M. Gorelick, and J. Caers (2008), Identifying discrete geologic structures that produce anomalous hydraulic response: An inverse modeling approach, *Water Resour. Res.*, *44*, W08426, doi:10.1029/2007WR006635.

Schad, H., and G. Teutsch (1994), Effects of the investigation scale on pumping test results in heterogeneous porous aquifers, *J. Hydrol.*, *159*, 61–77.

Sklar, A. (1959), Fonctions de répartition à n dimensions et leurs marges, *Publ. Inst. Stat. Paris*, *8*, 229–131.

Strebelle, S. (2002), Conditional simulation of complex geological structures using multiple-point statistics, *Math. Geol.*, *34*(1), 1–21.

Therrien, R., and E. A. Sudicky (1996), Three-dimensional analysis of variably saturated flow and solute transport in discretely-fractured porous media, *J. Contam. Hydrol.*, *23*, 1–44.

Wood, A. (1995), When is a truncated covariance function on the line a covariance function on the circle?, *Stat. Probab. Lett.*, *24*, 157–164.

Wood, A., and G. Chan (1994), Simulation of stationary Gaussian process in $[0, 1]^d$, *J. Comput. Graph. Stat.*, *3*, 409–432.

Zhang, T., P. Switzer, and A. Journel (2006), Filter-based classification of training image patterns for spatial simulation, *Math. Geol.*, *38*(1), 63–80, doi:10.1007/s11004-005-9004-x.

Zhou, H., J. J. Gómez-Hernández, H. Franssen, and L. Li (2011), An approach to handling non-Gaussianity of parameters and state variables in ensemble Kalman filtering, *Adv. Water Resour.*, *34*, 844–864.

Zhou, H., L. Li, H. Franssen, and J. J. Gómez-Hernández (2012a), Pattern recognition in a bimodal aquifer using the normal-score ensemble Kalman filter, *Math. Geosci.*, *44*, 169–185.

Zhou, H., J. J. Gómez-Hernández, and L. Li (2012b), A pattern-search-based inverse method, *Water Resour. Res.*, *48*, W03505, doi:10.1029/2011WR011195.

Zhou, H., J. J. Gómez-Hernández, and L. Li (2014), Inverse methods in hydrogeology: Evolution and recent trends, *Adv. Water Resour.*, *63*, 22–37, doi:10.1016/j.advwatres.2013.10.014.

Zinn, B., and C. Harvey (2003), When good statistical models of aquifer heterogeneity go bad: A comparison of flow, dispersion, and mass transfer in connected and multivariate Gaussian hydraulic conductivity fields, *Water Resour. Res.*, *39*(3), 1051, doi:10.1029/2001WR001146.